OPTIMIZING CNT-CROSSLINKS AND CNT CHIRALITY ON FIBER STRENGTH AND TOUGHNESS

Charles F. Cornwell, Charles R. Welch

Information Technology Laboratory
U.S. Army Engineer Research and Development Center
3909 Halls Ferry Road
Vicksburg, MS 39180
{Charles.F.Cornwell; Charles.R.Welch}@usace.army.mil

Keywords: load transfer, nanofibers, strength, crosslinks

Abstract
In this study, we report on atomistic simulations that show that optimizing the density of cross-links between CNTs can cause the response of the resultant fibers to transition from brittle to ductile behavior. Fiber response to tensile loads was calculated to reveal the effects these variations have on fiber properties.

1 Introduction

Military engineering and infrastructure engineering are heavily dependent on available materials and their rheological properties. These fields of engineering can be divided into three major areas: tactics/policy (what is to be done); processes/procedures (how it is to be done); and material and personnel resources (who/what is going to be used to do it). Material performance constrains tactics/policy and process/procedures in that these have to operate within the bounds that materials will support. Accordingly, drastic improvements in material performance will be a disruptive and positive force for infrastructure and military engineering.

It is well known that many materials exhibit enormous strength at the molecular or microscale. As these micromaterials are scaled to macrolevels, the well-accepted theory of dislocations and their effect on fracture, fatigue, and material failure comes into play and significantly degrades their strength. For example, in a classic paper, Brenner [1] performed experiments on microscale samples of common materials. Some of his results are provided in table 1. In his experiments, small-diameter single crystal whiskers of common materials such as copper, iron, and silver were subjected to tensile tests. These were found to exhibit ultimate tensile strengths many times the strength of the associated bulk materials. For example, the micro-whiskers of iron were found to have tensile strengths of about 1.9 million psi (13.1 GPa), whereas the maximum tensile strength for bulk iron ranges from 22.7 to 32.7 ksi, or only about 1 to 2 percent of that of the single crystal iron whiskers. Brenner found that as the length or diameter of the specimens increased for a given material, the tensile strength decreased. Fig. 1 [1] displays the tensile strength of iron whiskers of similar length as a function of 1/diameter of the whisker in which a linear relationship is inferred. The same

order strength degradation has been observed for other materials, and might be expected for carbon nanotube-based materials unless intelligent material design intercedes.

Table 1 Properties of Micro-Scale Samples of Common Materials		
Material	Diameter 10^{-6} m	Tensile Strength GPa
Iron	1.60	13.1
Copper	1.25	2.93
Silver	3.80	1.72

Table 1. Properties of Micro-Scale Samples of Common Materials

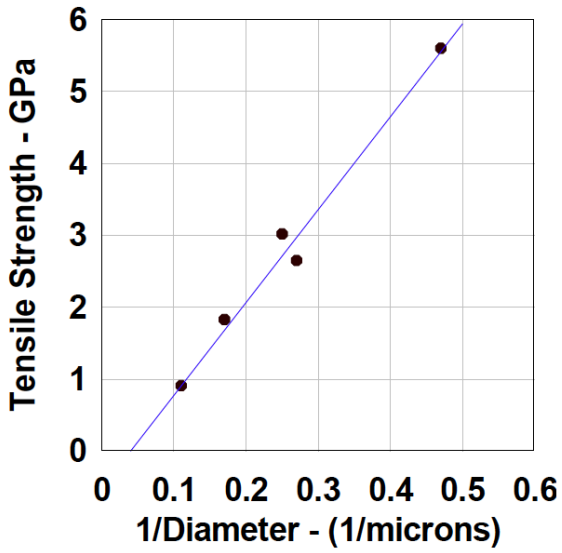

Figure 1. Tensile strength of iron whiskers of similar length [1].

The superior strength and stiffness of carbon nanotubes (CNTs) make them attractive for many structural applications. While the strength and stiffness of CNTs are extremely high, fibers of aligned CNTs have been found to date to be far weaker than the constituent CNTs [2-5]. The intermolecular interactions between the CNTs in the fibers are governed by weak van der Waals forces, resulting in slippage between CNTs that occurs at tensions well below the breaking strength of the CNTs. Both theoretical and experimental studies show that introducing chemical bonds between the CNTs increases load transfer and prevents the CNTs from slipping [6]. In this paper we describe the use of chemical bonds as an effective mechanism for coupling the superior mechanical properties of the individual CNTs across length scales. The results show an increase in the strength and elastic modulus of the fibers and also reveal a transition from ductile to brittle failure going from fibers with low to higher cross-link counts.

2 Fiber Construction

Experimental results indicate that CNTs within a bundle have similar radii and are randomly distributed [7]; i.e., there is no correlation between the longitudinal coordinates of the different tubes, and they most probably have random azimuthal orientations. The digital representations of the fibers were constructed using a random distribution of CNT lengths, with each CNT given a random rotation about its longitudinal axis between 0 and 2π. The longitudinal axes of the fibers were initially aligned parallel to the z-axis. The strands consisted of (5,5) CNTs placed end to end arranged parallel to one another with a gap of 3.33Å between CNTs in the strands (Fig. 2a). Each bundle had 19 strands arranged in a hexagonal close packed configuration (Fig. 2c).

The positions of the cross-link atoms were randomly selected from the volume of the bundle. A check was made to determine if the cross-link atom formed the correct number of nearest-neighbor bonds and that it formed bonds between CNTs from two different strands. If it did

not meet these criteria, it was rejected. The cross-links are formed by a single carbon atom placed in the interstitial region between the strands of the fiber (Fig. 2b). The concentration of cross-link atoms is defined as the number of cross-link atoms divided by the number of atoms in the bundle expressed as a percentage.

The simulations had periodic boundary conditions in the three Cartesian dimensions. The system size in the x-y plane was large enough to prevent any interaction across the boundary for atoms in the bundle. The simulations were carried out using Sandia Laboratory's Large-scale Atomic/Molecular Massively Parallel Simulator (LAMMPS) code [8]. The potential energy of the system was calculated using the Adaptive Intermolecular Reactive Empirical Bond Order (AIREBO) Potential [9]. Newton's equations of motion were numerically integrated over time using the Velocity-Verlet integrator [10] with a time-step of 1.0 femtoseconds.

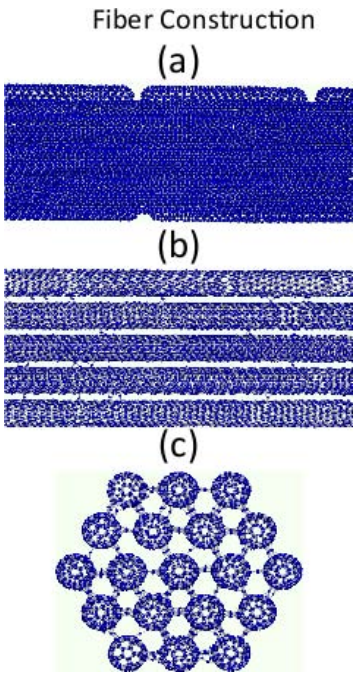

Figure 2. Carbon nanotube fiber (a) initial configuration with CNTs placed end-to-end over the length of the fiber; (b) interstitial carbon atoms forming cross-link bonds along the length of the fiber; (c) cross section of fiber with cross-link bonds between the

A Langevin thermostat [11] was applied to all the atoms to minimize the heat conduction problem pointed out in Berendsen et al. [12]. Mylvaganam and Zhang [13] and Ito et al. [14] examined the effect of various potentials and thermostat schemes, and both papers came to the same conclusion that all atoms in the system should be coupled to a thermostat. Ito et al. [14] examined the Langevin and Berendsen thermostats to simulate chemical reaction rates for chemical sputtering on graphite. Experimental results were accurately reproduced using the Langevin thermostat but not the Berendsen thermostat to control the temperature.

Cooling and heating by thermostats generally affect the rate of chemical reactions, and the Langevin and Berendsen thermostats cool or heat atoms by different mechanisms. The Berendsen thermostat can be regarded as a global thermostat where the velocity of the atoms is scaled based on the temperature of the entire system. On the other hand, the Langevin thermostat can be regarded as a local thermostat where the kinetic energy of each atom is scaled based on the instantaneous temperature of the individual atoms independent of the other atoms. The rate of chemical reactions generally depends on the kinetic energy of each atom rather than the temperature of the entire system. The local kinetic energy generated by exothermic reactions during fracture is absorbed by the Langevin thermostat and more accurately simulates heat conduction under experimental conditions. The simulations were run at a temperature of 300 K with a damping coefficient of 0.01 picoseconds (ps) [15].

The stress tensor was calculated using the following equation:

$$< S_{ij} > = \frac{\sum_{k}^{N} m_k v_{k_i} v_{k_j}}{V} + \frac{\sum_{k}^{N} r_{k_i} f_{k_j}}{V} \qquad (1)$$

The first term of Eq. (1) is the kinetic energy tensor, and the second term is the virial stress tensor. N is the number of atoms in the system, and the Cartesian coordinates are designated by i and j = x,y,z. The variables m_k, v_k, r_k, and f_k are the mass, velocity, position, and force, respectively, for atom k, and V is the volume of the bundle. Here, the volume of the bundle is calculated using the length of the bundle times its cross section. The area of a regular hexagon that encloses the strands of the bundle is used to define the cross-sectional area of the fiber. Figure 2c shows the cross section of the fibers with the cross-link atoms forming chemical bonds between the CNTs. The cross-section of the bundle is considered constant throughout the simulation.

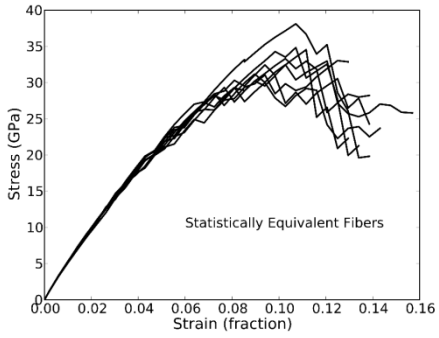

Figure 3. Stress-strain curves for eight statistically equivalent fibers. A different seed is used for the random number generator to construct the fiber. All of the fibers are 4000 Å long and are constructed using CNTs with an average length of 1000 Å with a standard deviation in the tube length of 200 Å.

Because the fibers were constructed using CNTs with random orientations, random distribution of lengths, and a random distribution of cross-link atoms, one would expect variations in the mechanical properties of the fibers caused by the random method of fiber construction. Figure 3 shows the stress-strain curves for eight statistically equivalent fibers. The fibers were 4000 Å long and were constructed using CNTs with an average length of 1000 Å. The standard deviation in the tube length was 200 Å, and they all had a cross-link concentration of about 0.225%. The average maximum stress for the eight simulations was 33.467 GPa with a standard deviation of 2.495 GPa. This represents a standard deviation of 7.46% of the average maximum stress. The eight simulations had an average initial elastic modulus of 586.434 GPa with a standard deviation of 14.743 GPa representing a standard deviation of 2.51% of the average initial modulus. While there are some variations in the stress-strain curves in fig. 3, the simulations produce consistent and reproducible results for statistically equivalent fibers. This indicates that the time-average of the stress-strain curves and the CNT ensembles used to construct the fibers were generally adequate to average out the statistical variations in the mechanical properties caused by the random fiber construction process. Trends in fiber properties can be determined because the statistical variations in the fiber properties were small compared to the effects due to variations in CNT length and cross-link distribution. To minimize the effects of statistical variations, the same seed for the random number generator was used to construct all of the remaining fibers.

3 Results

A series of simulations were run to investigate the effect of CNT length and cross-link distribution on the tensile response of parallel-aligned CNT fibers. Figure 4 shows the tensile stress-strain plots

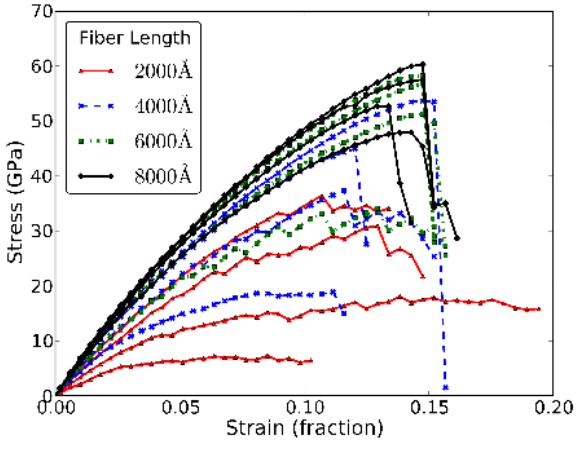

Figure 4. Simulation stress-strain curve results for fiber lengths of 2000, 4000, 6000, and 8000Å with initial cross-link concentrations of 0.125, 0.250, 0.500, and 0.750 percent. The plots of lower to higher cross-link concentrations run from lower to higher stress for each fiber length considered.

for fibers with initial lengths of 2000, 4000, 6000, and 8000Å. In each case, the initial fiber length was 4 times the average CNT length, and the standard deviation in the CNT length was 0.2 times the average CNT length. The maximum stress for each fiber length increased with an increase in the concentration of cross-link atoms. From the results of the stress-strain calculations presented in Fig. 4, the overall trends of the elastic modulus, tensile strength, and critical strain, that is failure strain, for fibers of different lengths and concentrations of cross-links are visible. The elastic modulus was calculated over the linear portion of the stress-strain curves, hence is an initial or tangent modulus. The point of maximum stress was used to determine the tensile strength of the fibers. The critical strains ranged from 0.085 for the 2000Å fiber with an initial cross-link concentration of 0.125 percent, to a critical strain of 0.148 for the 6000Å fiber with an initial cross-link percentage of 0.500. The maximum tensile strength and elastic modulus of 62.3 and 721.2 GPa, respectively, were calculated for the 8000Å-long fiber with a percentage of cross-links of 0.750. The tensile strength of the (5,5) CNTs used to construct the fibers is 110 GPa [16]. The calculations presented herein indicate that the load transfer provided by the cross-link atoms allows the fiber to retain a substantial portion of the strength of the constituent CNTs in the fiber. The elastic modulus, tensile strength, and critical strain increased with increasing CNT length and cross-link concentration, with both the elastic modulus and tensile strength approaching an asymptotic limit. The trends in the elastic modulus and fiber strength for each fiber length are also apparent when calculated for the different cross-link concentrations.

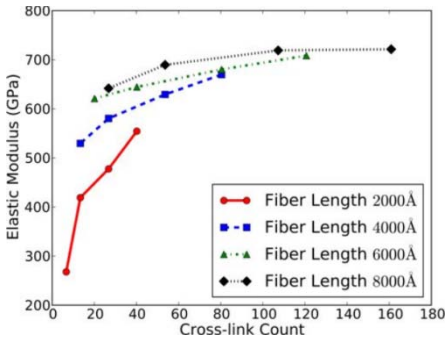

Figure 5. Elastic modulus for fibers 2,000, 4,000, 6,000, and 8,000Å long versus approximate average number of cross-links

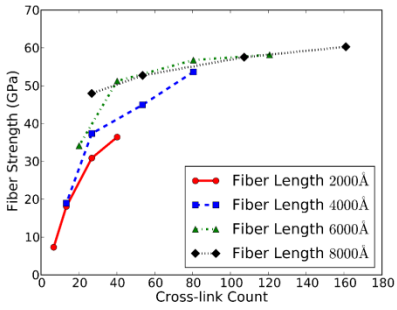

Figure 6. Fiber strength for fiber lengths of 2,000, 4,000, 6,000, and 8,000Å with increasing cross-link concentrations.

The effect of interstitial carbon atom cross-linking on the properties of CNT fibers can be better understood by considering the average number of cross-links per CNT. Figures 5 and 6 show the elastic modulus and fiber strength as a function of the average number of cross-links for the core CNTs in the fibers. For this range of parameters, Figs. 5 and 6 indicate that the elastic modulus and fiber strength of the shorter fibers depend on both the average length of the constituent CNTs and the average number of cross-links per CNT. The dependence of the mechanical properties of the fiber on the average CNT length is largest for short fibers with low cross-link counts. For fibers with higher cross-link counts, the elastic modulus and fiber strength depend on the cross-link count and are far less dependent on the average length of the constituent CNTs. In Fig. 6, fibers 4000, 6000, and 8000Å long with a cross-link count of 80 have strengths that range from 53.7 GPa to 56.8 GPa. Both the elastic modulus and fiber strength approach an asymptotic limit with increased cross-link counts. The results also indicate that it is possible to reach the maximum values for both the elastic modulus and fiber

strength with lower cross-link counts for fibers constructed with longer CNTs. It may also reflect the fact that to have the same number of cross-links for the shorter CNTs requires cross-links closer to each other in the CNTs. This may weaken the CNTs as the bonding structure goes from a 3-coordinated carbon-carbon bond to a 4-coordinated carbon-carbon bond. Fig. 4 suggests a transition from ductile to brittle behavior going from fibers constructed from the shorter CNTs and low cross-link counts to fibers constructed from longer CNTs and higher cross-link counts, that is, as the number of cross-links per CNT increased.

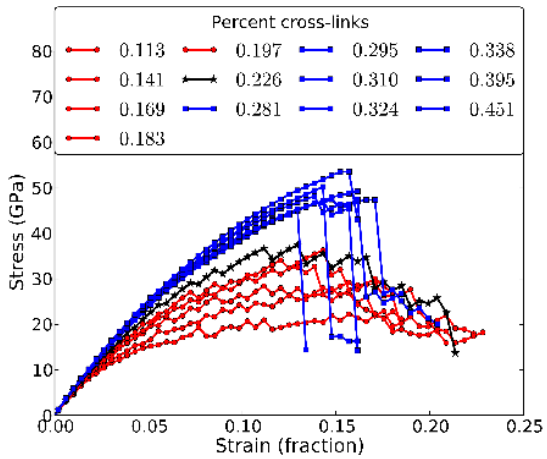

Figure 7. Stress-strain curves for a bundle 4000Å long with the percent cross-links ranging from 0.113 to 0.451.

A detailed understanding of the bundle post-yield response is required to optimize the strength and elastic modulus of fibers and to prevent brittle failure. A series of simulations were run to investigate the effect of CNT cross-link concentrations on the post-yield response of parallel-aligned CNT fibers. Results of the stress-strain calculations are presented in Fig. 7. Data from the stress-strain calculations are used to determine the elastic modulus and tensile strength for fibers with initial lengths of 4000 Å with cross-link concentrations that ranged from 0.113 to 0.451 percent. The plots of lower to higher cross-link concentrations ran from lower to higher stress for each cross-link concentration considered. The maximum tensile strength of 50.24 GPa was calculated for the bundle with an initial percentage of cross-links of 0.395, and the maximum elastic modulus of 629.17 GPa was calculated for the bundle with an initial percentage of cross-links of 0.451. The results of the stress-strain calculations presented in Fig. 7 also reveal a transition from ductile to brittle failure going from bundles with low to higher cross-link counts. Figure 4 shows a transition from ductile to brittle between cross-link concentrations of 0.226. and 0.281 percent.

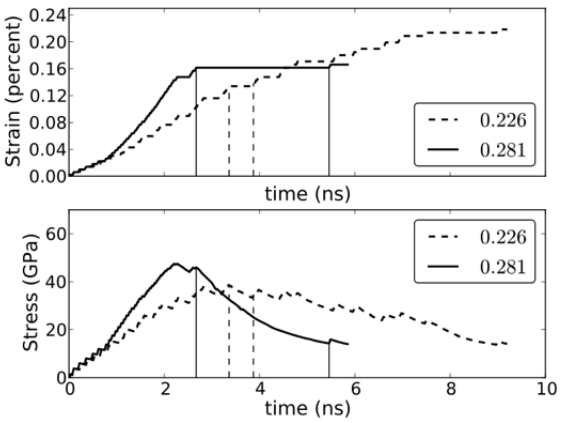

Figure 8. Time evolution of the stress and strain for a 4000Å bundle. The average length of the CNTs in the bundle is 1000Å with a standard deviation of 200Å. The initial percentages of cross-links in the fibers are 0.226 and 0.281.

The results in Fig. 8 show the time evolution of the stress and strain for two 4000 Å fibers. The average length and standard deviation of the CNTs in both fibers are 1000 Å and 200 Å, respectively. The number of cross-links per CNT in the two fibers differs. The initial percentage of cross-links is 0.226 and 0.281 or an average of 26.8 and 33.4 cross-links for each core CNT, respectively. From Fig. 4, these two plots have the highest cross-link concentration (0.226) that exhibits ductile post-yield behavior and the lowest cross-link concentration (0.281) that exhibits brittle post-yield behavior and are used to examine the brittle and ductile response of the fibers. The plot of the stress and strain

data in Fig. 8 is the time average of the stress and strain at 10-ps intervals.

In Fig. 8 the bundle with 0.281 percent cross-link concentration reached a maximum stress of 47.49 GPa at a strain of 0.148 in 2.27 nanoseconds (ns). On the other hand, plot 0.226 in Fig. 8 reached a maximum stress of 38.67 GPa at a strain of 0.134 in 3.35 ns. Generally, the fibers with shorter CNTs and lower concentrations of cross-links fail at the cross-links. Apparently, failure of a cross-link results in less damage to the CNTs and thus in very little damage to the bundle. The simulations indicate that failure in all fibers begins when the bundle responds to bond breaking, defect formation, and slipping or failure of the CNTs. Recall that displacement boundary conditions were used in the simulations. While the average strain in the bundle was holding constant, inside the bundle, bonds were failing and the average internal stress was decreasing. This results in a release of stress and structural changes in the bundle. If the resulting structure of the bundle is able to support the residual stress, the stress stabilizes. Otherwise, the bundle fails again and the process is repeated until the stress stabilizes or the bundle breaks. Figures 9 and 10 capture snapshots of the post-yield results of bundle failure.

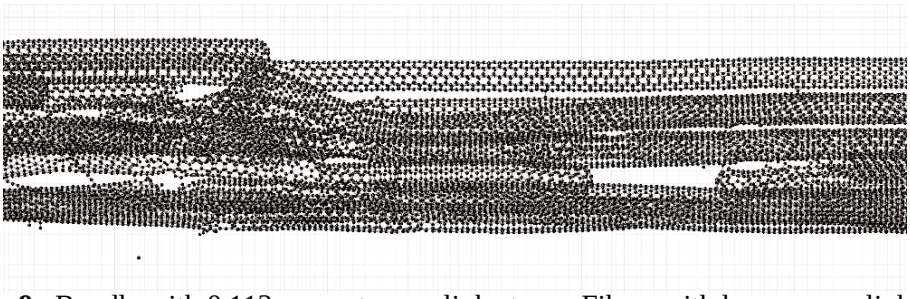

Figure 9. Bundle with 0.113 percent cross-link atoms. Fibers with lower cross-link concentrations tend to achieve lower maximum stress but produce less damage to the bundle during failure. As a result, the failure tends to be more ductile.

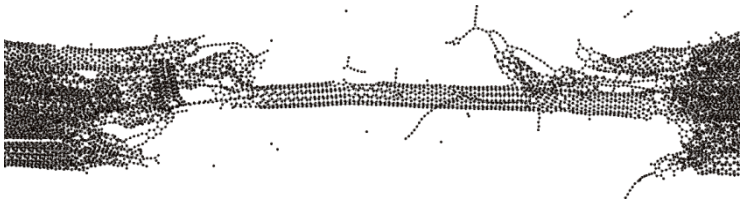

Figure 10. Bundle with 0.394 percent cross-limk atoms. Fibers with higher cross-link concentrations tend to achieve higher maximum stress but produce substantial damage to the bundle during failure. As a result, the failure tends to be brittle.

Conclusion

These results indicate that cross-links between CNTs promote load transfer while allowing them to retain the majority of their structural integrity. Such cross-linking would allow a CNT fiber to be constructed with theoretical strengths, if composed of chiral (5,5) CNTs, of approximately 60 GPa. The simulations show an increase in the elastic modulus, critical strain, and yield strength with an increase in cross-link concentrations. The results also demonstrate that fibers constructed with longer CNTs achieve maximum tensile strength with lower cross-link concentrations. Taken together, the results suggest that the average number of cross-links per molecule is the controlling factor, with perhaps a smaller effect being the proximity of cross-links within a CNT causing a slight weakening of the CNT. The simulations showed that the fibers with lower cross-link concentrations failed at the C-C bonds of the cross-link atoms. This allowed the CNTs to slip past one another and in general tended to produce less damage to the bundle, resulting in a ductile response. On the other hand, the CNTs tended to fail in fibers with higher concentrations of cross-links. A CNT

failure damages the bundle and makes it less likely that it will be able to support the residual stress in the bundle resulting in brittle failure. Precise control of the cross-link concentration and distribution may allow the maximum bundle strength and elastic modulus to be achieved while producing favorable post-yield behavior. Ultimately, the ability to produce CNT fibers with a minimum number of defects while optimizing the number and distribution of cross-links will play a major roll in determining the properties of CNT fibers.

References

[1] Brenner, S. S., Tensile strength of whiskers. Journal of Applied Physics, **27**, 1484-1491 (1956).
[2] D. Qian, W. K. Liu, and R. S. Ruoff, *Load transfer mechanism in carbon nanotube ropes*, Compos. Sci. Technol. **63**, 1561 (2003)
[3] L. M. Ericson, H. Fan, H. Peng, V. A. Davis, W. Zhou, J. Sulpizio, Y. Wang, R. Booker, J. Vavro, C. Guthy, A. N. G. Parra-Vasquez, M. J. Kim, S. Ramesh, R. K. Saini, C. Kittrel, G. Lavin, H. Schmidt, W. W. Adams, W. E. Billps, M. Pasquali, W. F. Hwang, R. H. Hauge, J. E. Fischer, R. E. Smalley, *Macroscopic, neat, single-walled carbon nanotube fibers*, Science **305**, 1447 (2004).
[4] K. Koziol, J. Vilatela, A. Moisala, M. Motta, P. Cunniff, M. Sennett, and A. Windle, *High-performance carbon nanotube fiber*, Science **318**, 1892 (2007).
[5] S. Zhang, L. Zhu, M. L. Minus, H. G. Chae, S. Jagannathan, C.-P. Wong, J. Kowalik, L. B. Roberson, and S. Kumar, *Solid-state spun fibers and yarns from 1 mm long carbon nanotube forests synthesised by water-assisted chemical vapour deposition*, J. Mater. Sci. **43**, 4356 (2008).
[6] A. V. Krasheninnikov and K. Nordlund, Ion and electron irradiation-induced effects in nanostructured materials, J. Appl. Phys. **107**, 071301 (2010).
[7] A. Thess, R. Lee, P. Nikolaev, H. Dai, P. Petit, J. Robert, C. Xu, Y. H. Lee, S. G. Kim, A. G. Rinzler, D. T. Colbert, G. E. Scuseria,D. Tomanek, J. E. Fischer, R. E. Smalley, *Crystalline ropes of metallic carbon nanotubes*, Science, **273**, 483 (1996).
[8] S. J. Plimpton, *Fast parallel algorithms for short-range molecular dynamics*, J. Comp. Phys., **117**, 1, (1995).
[9] J. S. Stuart, A. B. Tutein, and J. A. Harrison, *A reactive potential for hydrocarbons with intermolecular interactions,* J. Chem. Phys, **112**, 6486 (2000).
[10] L. Verlet, *Computer 'experiments' on classical fluids. II Equilibrium correlation functions,* Phys. Rev., **159**, 98, 1967.
[11] T. Schneider, and E. Stoll, Molecular dynamics study of three-dimensional one-component model for distortive phase transitions, Phys Rev B, **17**, 1302 (1978).
[12] H. J. C. Berendsen, J. P. M. Postma, W. F. van Gunsteren, A. DiNola, and J. R. Haak, Molecular dynamics with coupling to an external bath, J. Chem. Phys. **81**, 3684 (1984).
[13] K. Mylvaganam and L. C. Zhang, Important issues in a molecular dynamics simulation for characterising the mechanical properties of carbon nanotubes, Carbon **42**, 2025 (2004).
[14] A. M. Ito, H. Okumura, S. Saito, and H. Nakamura, Examination of temperature dependence of chemical sputtering on graphite by comparing the Langevin and Berendsen Thermostats, Plasma and Fusion Research 5, S2020-1 (2010)
[15] P. Xiu, B. Zhou, W. Qi, H. Lu, Y. Tu, and H. Fang, *Manipulating biomolecules with aqueous liquids confined within single-walled nanotubes*, J. Am. Chem. Soc. **131,** 2841 (2009)
[16] R. W. Haskins, R. S. Maier, R. M. Ebeling, C. P. Marsh, D. L. Majure, A. J. Bednar, C. R.Welch, B. C. Barker, and D. T.Wu, J. Chem. Phys. **127**, 074708 (2007).